Vol. 46, No. 3 (2024) 379-397, DOI: 10.24874/ti.1570.11.23.01

Tribology in Industry

www.tribology.rs

RESEARCH

Investigation on Microstructures, Hardness, Friction, and Wear of Cold Sprayed Ti6Al4V Coatings With Coating Thickness of 100-3000 µm

Nay Win Khun[a,b]*, Adrian Wei Yee Tana[a,b], Wen Sun[a,b], Erjia Liu[a,b]

[a]*School of Mechanical and Aerospace Engineering, Nanyang Technological University, 50 Nanyang Avenue, Singapore,*
[b]*Rolls-Royce@NTU Corporate Laboratory, Nanyang Technological University, Singapore.*

Keywords:

Cold spray
Ti-6Al-4V
Coatings
Thickness
Hardness
Wear

* Corresponding author:

Nay Win Khun
E-mail: khunnaywin@gmail.com

Received: 3 November 2023
Revised: 20 December 2023
Accepted: 15 January 2024

A B S T R A C T

The effect of coating thickness (CT) on the microstructures, hardness, and wear of cold sprayed Ti-6Al-4V (CS-Ti64) coatings was systematically investigated since the prolonged high pressure CS deposition could change their microstructures and porosity levels. In addition, the CT was relatively important for their durability, performance, and service life. Therefore, the CS-Ti64 coatings with different CT of 100-3000 µm were prepared on commercially available Ti64 (CA-Ti64) substrates via high pressure CS processes. The CS-Ti64 coatings had low porosity levels wherewith severely deformed Ti64 particles with a crescent-shape could be seen in their cross-sectional microstructures. The hardness of the CS-Ti64 coatings increased with increased CT probably due to their lowered bulk porosity levels associated with longer high pressure CS deposition. As a result, the increased CT from 100 to 3000 µm resulted in a 9.8% decrease in the wear of the CS-Ti64 coatings. The wear of the CS-Ti64 coating with 3000 µm was 16.8% lower than that of the CA-Ti64 as all the CS-Ti64 coatings had lower wear than the CA-Ti64. It could be concluded that the prolonged high pressure CS deposition for the thick CS-Ti64 coatings had an influence on their porosity, hardness, and wear .

1. INTRODUCTION

In the aircraft industry, the use of low temperature CS technology has become a potentially important strategy to replace high temperature thermal spray (TS) technologies, which are widely used in the repair industry, for repair of heat sensitive aerospace components (ACs) [1-3]. Compared to high temperature TS technologies, low temperature CS technology can be used to build metallic coatings with lower porosity and oxidation levels, lack of thermal residual stress, and higher possibility to achieve high CT [4]. Pitchuka et al. [5] investigated the tribological properties of CS-aluminium alloy coatings with better tribological performance than commercial AA-6061. Although the enhanced abrasive wear resistance of CS-metallic

coatings has been found by some researchers [2,6], the tribological data of CS-metallic coatings are not widely available due to the private nature and development stage of CS technology.

Ti64, which is a widely used aerospace material with light weight, high strength, and so on, has poor abrasive wear resistance so that expensive ACs made of it demand repair during their long-service [2,3,7]. Therefore, CS technology can be used to repair wear damages of Ti64 based ACs because the use of CS technology is beneficial in repairing ACs with built Ti64 that has higher abrasive wear resistance than CA-Ti64 [2]. The thickness of built metallic materials should be taken into account for repair applications because a prolonged high pressure CS deposition can change their microstructures and porosity levels, thereby hardness and wear resistance [8,9]. Moridi et al. [9] investigated the mechanical properties of CS-AA6082 coatings with different CT. Xiong et al. [10] studied the effect of CT on the bond strength of CS-AA7075 and 7050 coatings. Khun et al. [11] investigated the tribological properties of CS-Ti coatings with different CT. Since there is a difference in the hardness of spray Ti and Ti64 particles, their different adiabatic shear deformation during CS deposition can give rise to significant differences in the microstructures and thereby the mechanical and tribological properties of CS-Ti and CS-Ti64 coatings. However, a thorough investigation on the friction and wear of CS-Ti64 coatings with different CT has not been widely reported in the literature yet and is still necessary since a scientific understanding of the process-structure-property relationships of CS-Ti64 coatings is relatively important for their successful repair applications.

In this study, the CS-Ti64 coatings with different CT of 100-3000 μm were prepared on the CA-Ti64 substrates using a 5/11 CS system to investigate the effect of CT on their microstructures, hardness, friction, and wear. Their detailed microstructures were carefully examined via optical microscopy (OM) as their hardness was thoroughly analysed with a Vickers micro-indenter. Their friction and wear against 100Cr6 steel under a dry condition were comparatively investigated with ball-on-disc tribo-tests by performing a systematic correlation between their CT and tribological performance. The CA-Ti64 was used as a reference material.

2. EXPERIMENTAL DETAILS

2.1 Sample preparation

Feedstock material of spherical Ti64 powder (ASTM B348 Grade 23, apparent density: 2.5 g/cm^3) with a size distribution of 15-45 μm (Figure 1), but with some satellites, was purchased from Advanced Powders and Coatings Inc., Canada to prepare the CS-Ti64 coatings. Grade-5 CA-Ti64 plates with 50 mm × 50 mm × 8 mm (Titan Singapore) were used as substrates.

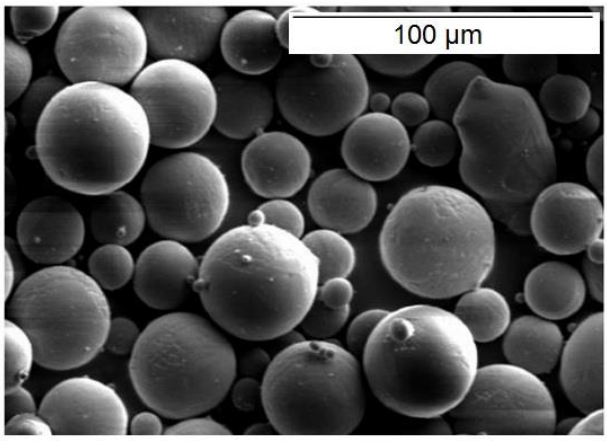

Figure 1. Overview of spray Ti64 powder used for CS-Ti64 coatings.

The machined CA-Ti64 substrates (Figure 2) were used instead of the sand blasted CA-Ti64 substrates to eliminate the negative effect of stuck sand particles on the coating bond strength.

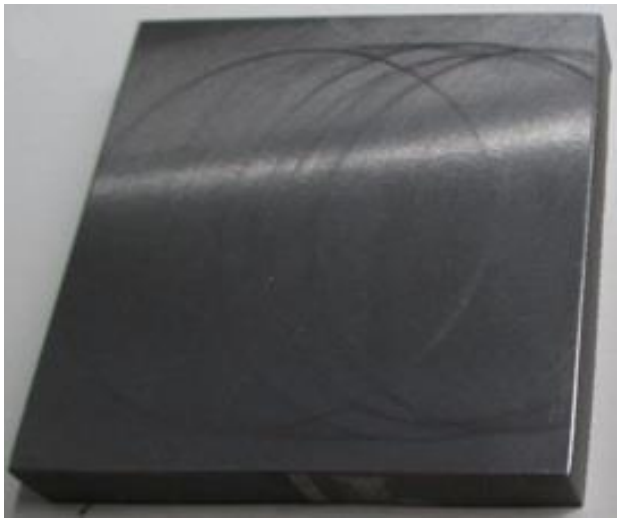

Figure 2. Overview of machined CA-Ti64 substrate.

The CS-Ti64 coatings with different CT of 100-3000 μm were deposited on the CA-Ti64 substrates using a 5/11 CS system (Impact

Innovation) (Figure 3) with nitrogen (N_2) working gas at working gas pressure and temperature of 4.8 MPa and 1100 °C, respectively, sample stage traverse speed of 500 mm/s, spray angle of 90°, raster step of 1 mm and stand-off distance of 30 mm.

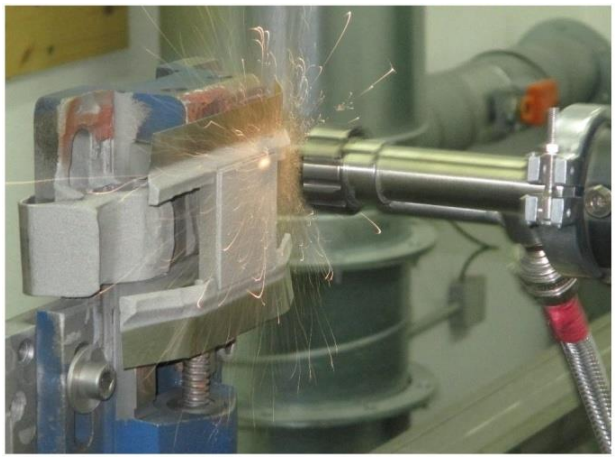

Figure 3. CS deposition of a CS-Ti64 coating using a 5/11 CS system.

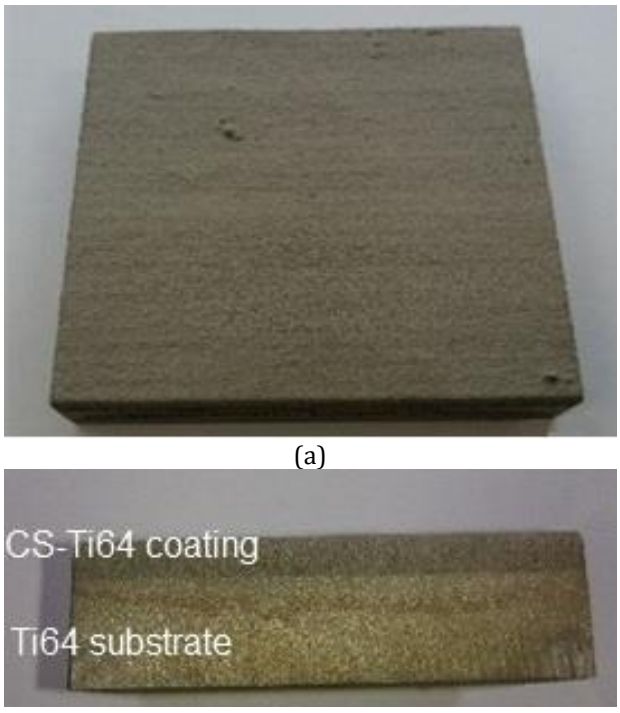

(a)

(b)

Figure 4. (a) Top and (b) cross-sectional views of as-deposited CS-Ti64-3000.

The CS-Ti64 coatings with CT of 100, 500, 1000 and 3000 μm on the machined CA-Ti64 substrates were assigned as CS-Ti64-T100, CS-Ti64-T500, CS-Ti64-T1000, and CS-Ti64-T3000, respectively. Figures 4a and b show the CS-Ti64-T3000 with a relatively uniform thickness.

2.2 Characterization

The CA-Ti64 substrate and CS-Ti64 coatings were systematically characterized as described below.

Their surface and wear topographies were obtained using surface profilometry (Talyscan 150) with a 4 μm diamond stylus. Their surface roughness was measured in terms of root mean squared surface roughness, R_q, that was sensitive to surface valleys and pores, and averaged from three random measurements on each sample.

Their surface and wear morphologies were observed via scanning electron microscopy (SEM, JEOL-JSM-5600LV).

Their crystalline structures were evaluated using a Philips MPD 1880 X-ray diffractometer (XRD) with a Cu-Kα radiation source powered with 40 kV and 30 mA.

Their microstructures and wear morphologies were captured via OM (Zeiss Axioskop 2, JVC color video camera). The CS-Ti64 coated samples were first moulded with two-component liquid epoxy in circular shaped Teflon molds with 25 mm diameter and 15 mm thickness, which were cured at room temperature (RT ~ 22-24 °C) for one day and then mechanically ground using 320 grit papers followed by chemical mechanical polishing with a (9 μm diamond particles) DiaPro solution and a (0.04 μm colloidal silica particles) OP-S suspension solution. At the final stage, their mirror-like surfaces were etched with Kroll's reagent to evaluate their detailed microstructures.

Their cross-sectional (bulk) porosity levels were obtained by analysing their OM micrographs, captured with 5×lens before etching, with Image "J" software and averaged with six OM micrographs per sample.

The chemical structures of their wear debris were analysed via X-ray photoelectron spectroscopy (XPS) (Kratos Axis Ultra) with a monochromatic Al Kα radiation source (hυ = 1486.71 eV) powered with 10 mA and 15 kV. A pass energy of 40 eV was used for the detail scans of C 1s, O 1s, Ti 2p, and Al 2p.

Their surface hardness was measured using a Vickers micro-indenter (Future-tech FM-300e) under an applied normal load of 200 g (1.96 N) and averaged from ten random indentations on each sample. Their cross-sectional hardness was measured along their thickness and averaged from three random indentations per line (the CT was systematically divided by many lines parallel to the substrate/coating interface with an equal distance and the cross-sectional hardness was measured along the line with three random indentations).

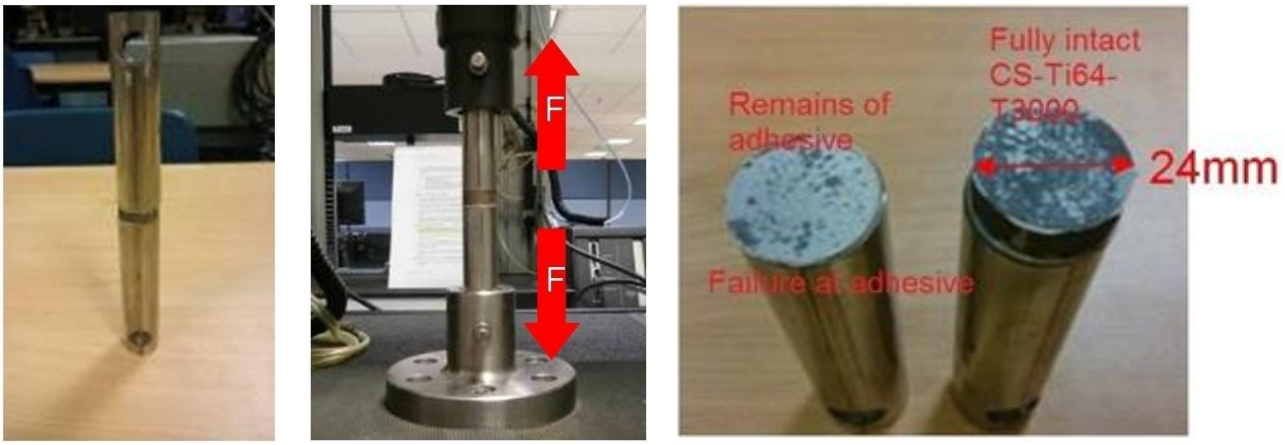

(a) (b) (c)

Figure 5. (a) Assembled set including CS-Ti64-T3000 coated sample bonded with two fixtures using adhesive glue before test, (b) tensile bond strength test, and (c) disassembled set with adhesive failure only at adhesive after test.

Their adhesion strength was evaluated according to the ASTM-C633 standard. The CS-Ti64 coated samples were wire-cut to get 24 mm circular buttons. Then, the surfaces of the buttons and fixtures were ground and cleaned with ethanol to be assembled together with Araldite AV170 adhesive glue (Huntsman Advanced Materials, USA) followed by curing at 150 ˚C for 60 min (Figure 5a). The assembled sets were tested using an universal tensile test (Instron 5569) with a 50 kN load cell at an extension rate of 0.8 mm/min (Figure 5b). The disassembled sets failed only at an adhesive after the tests as shown in Figure 5c.

Their topmost surface layers were carefully polished, especially for the thicker coatings, prior to the tribological test in order to eliminate the effect of their highly porous topmost surface layers on their friction and wear since the CS coatings always had the highest porosity levels at their topmost surface layers.

Their friction coefficients were measured with ball-on-disk tribo-tests (CSM Instruments) conformed to DIN50324 and ASTM G99. The polished CS-Ti64 and CA-Ti64 samples were rotated against fixed 6 mm 100Cr6 steel balls in a circular-path of 1 mm in radius for 30,000 laps at a sliding speed of 3 cm/s under an applied load of 1 N at RT. Their specific wear rates were obtained by measuring their wear widths and depths via surface profilometry to calculate their wear volumes and then dividing the wear volumes with the product of normal load and sliding distance. Their friction coefficients and specific wear rates were averaged from three random measurements per sample.

3. RESULTS AND DISCUSSION

3.1 Analysis of surface morphologies and topographies

The R_q values of the as-deposited CS-Ti64-T100, CS-Ti64-T500, CS-Ti64-T1000, and CS-Ti64-T3000 are 11.6±0.1 μm, 15.4±0.9 μm, 19.2±1.4 μm, and 57.1±7.2 μm, respectively. It is clear that the surface roughness of the CS-Ti64 coatings becomes higher with higher CT, especially for the CT of 3000 μm with a dramatic increase in the R_q value. Figures 6a and b show that the CS-Ti64-T3000 has a much rougher surface topography than the CS-Ti64-T100 probably due to the more localized

agglomeration of sprayed Ti64 particles with longer CS deposition [12,13]. During the CS process, a conversion of a major fraction of impact energies of spray Ti64 particles into heat causes them severely deformed under the adiabatic shearing conditions [14-16]. The possible accumulation of surface heat that does not dissipate promotes particle adhesion so that spray Ti64 particles flying even at low velocities below critical velocities can deposit with a less plastic deformation and a significant accumulate, which becomes pronounced with longer high pressure CS deposition and thereby results in the much higher surface roughness of the CS-Ti64-T3000 (Figure 6b) [14-16].

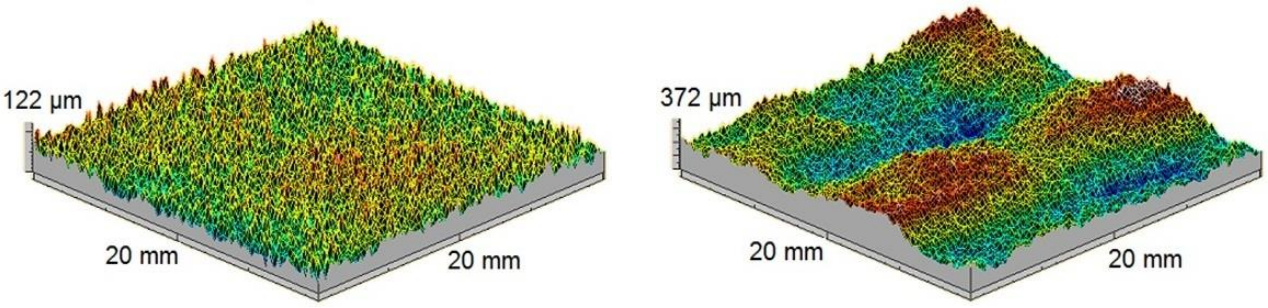

(a) (b)

Figure 6. Surface topographies of as-deposited (a) CS-Ti64-T100 and (b) CS-Ti64-T3000.

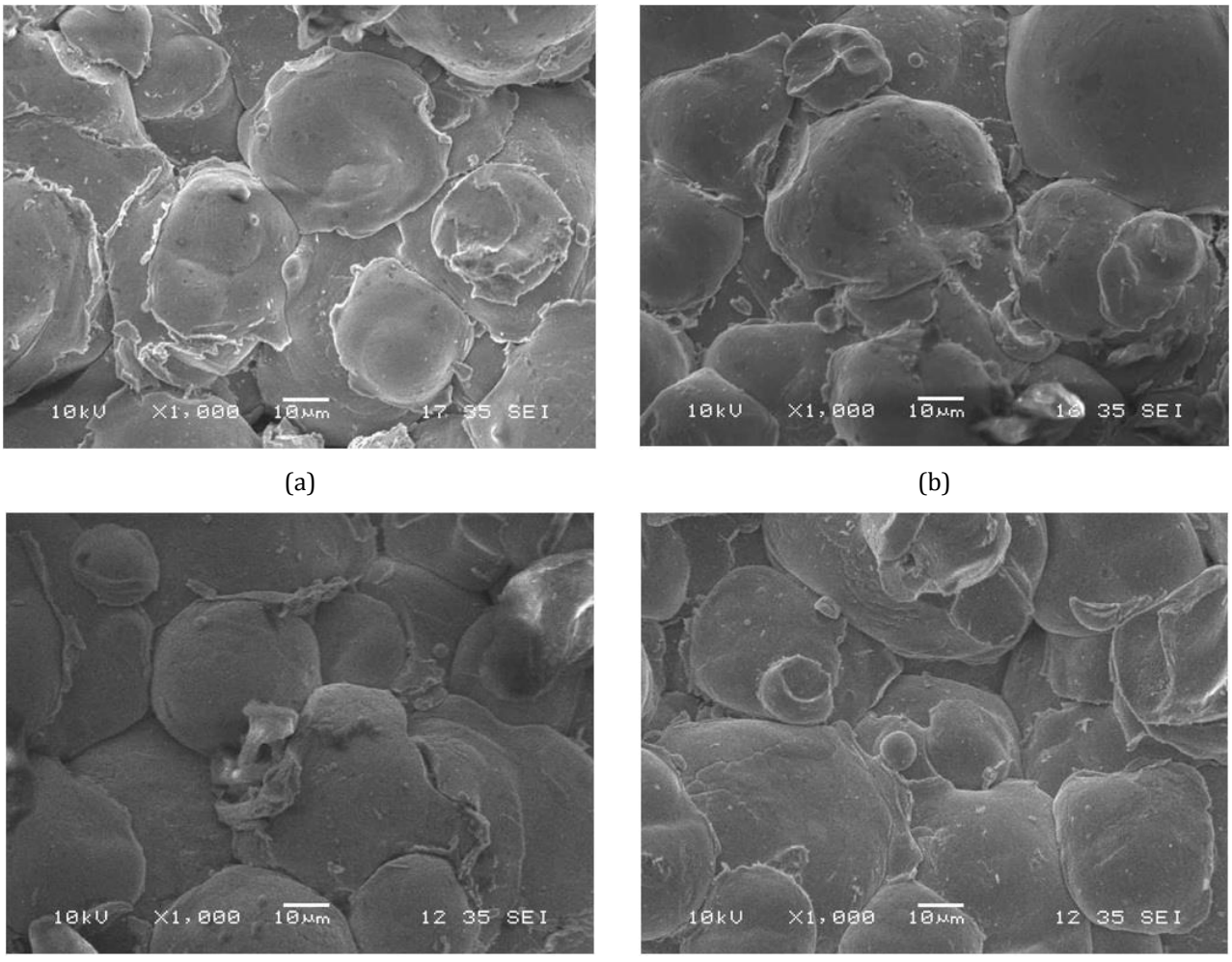

(a) (b)

(c) (d)

Figure 7. Surface morphologies of as-deposited (a) CS-Ti64-T100, (b) CS-Ti64-T500, (c) CS-Ti64-T1000, and (d) CS-Ti64-T3000.

Figure 7 shows the surface morphologies of the as-deposited CS-Ti64 coatings with different CT. Flattened Ti64 particles are indicative of their severe adiabatic shear deformation during the CS deposition as an intimate contact between them indicates their relatively strong bonding each other. The CS-Ti64-T1000 and CS-Ti64-T3000 (Figures 7c and d) have less severity of plastic deformation of sprayed Ti64 particles in their surface morphologies than the CS-Ti64-T100 and CS-Ti64-T500 (Figures 7a and b) because the higher accumulation of surface heat with longer high pressure CS deposition allows spray Ti64 particles to deposit on the surfaces with less plastic deformation [14-16].

3.2 Analysis of surface and cross-sectional microstructures

Figure 8a shows the surface microstructure of the CA-Ti64 on which a lamellar structure with α+β phases is found [17]. Elongated grains can be clearly seen in its cross-sectional microstructure as shown in Figure 8b.

Figure 9 shows the surface microstructures of the CS-Ti64 coatings with different CT. The sprayed Ti64 particles have visible interfaces, irregular shapes due to their severe plastic deformation, and intimate contact and locking each other. Unfilled gaps between sprayed Ti64 particles during the CS deposition are left as pores in their surface microstructures as found in Figure 9. They all have a certain number of pores in their surface microstructures.

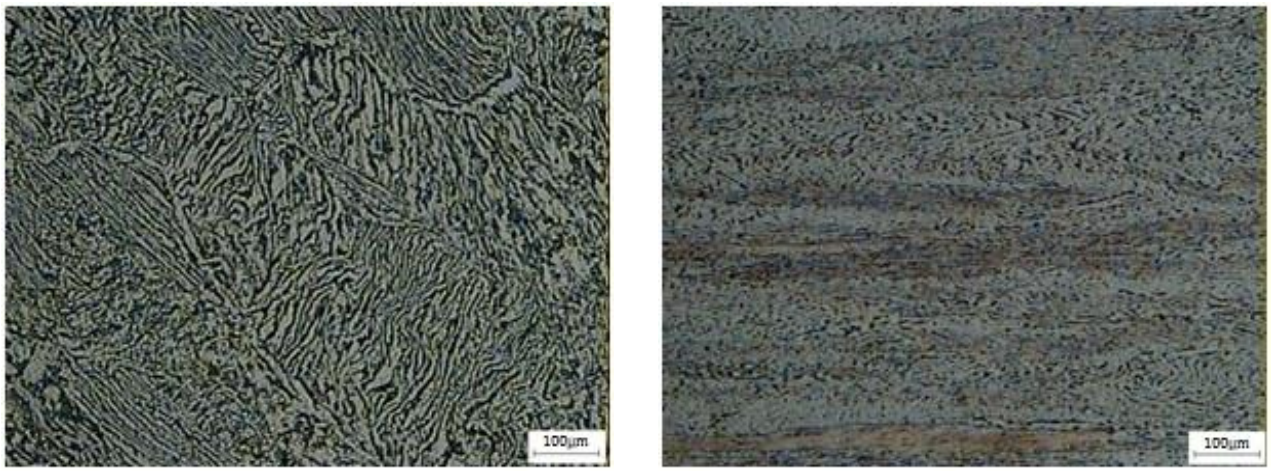

(a) (b)

Figure 8. (a) Surface and (b) cross-sectional microstructures of CA-Ti64.

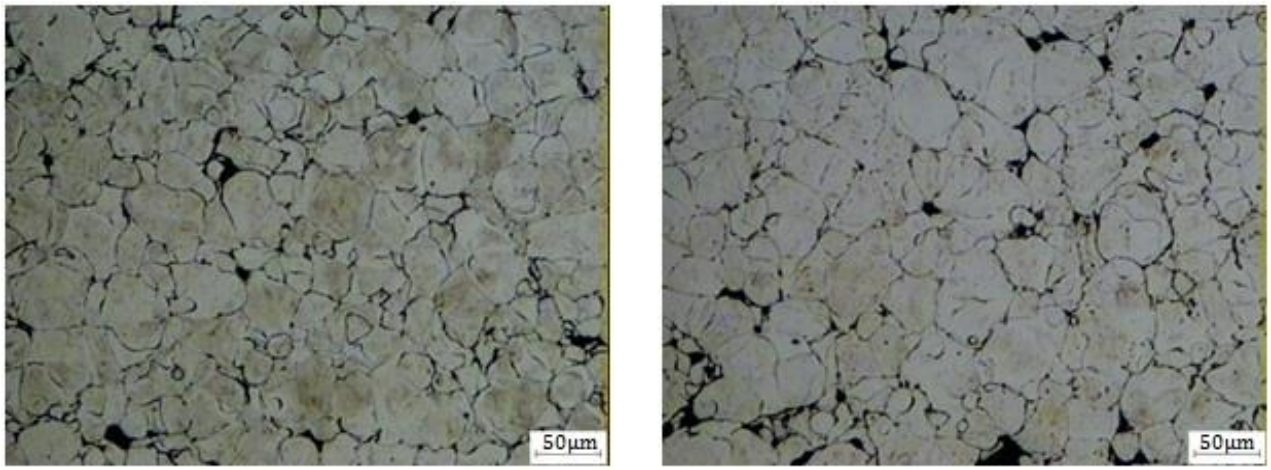

(a) (b)

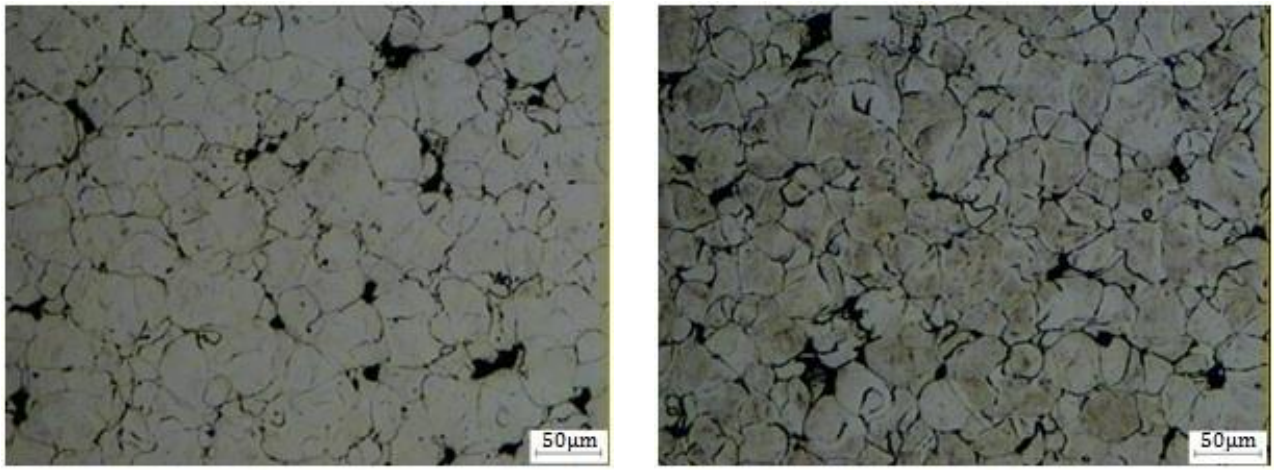

(c) (d)

Figure 9. Surface microstructures of (a) CS-Ti64-T100, (b) CS-Ti64-T500, (c) CS-Ti64-T1000, and (d) CS-Ti64-T3000.

In Figure 10, the XRD pattern of the CA-Ti64 with α-100, α-002, α-101, α-102, α-110, α-103, α-112, α-201, α-004 and β-200 peaks represents its lamellar structure with α+β phases (Figure 8a) [18,19]. β phases are not clearly identified in the XRD pattern of the CA-Ti64-T100 (Figure 10). The similar XRD patterns of the Ti64 powder and CS-Ti64-T100 are a confirmation of the CS-Ti64 coatings as well as an indication of no significant phase transformation of the Ti64 powder during the CS deposition.

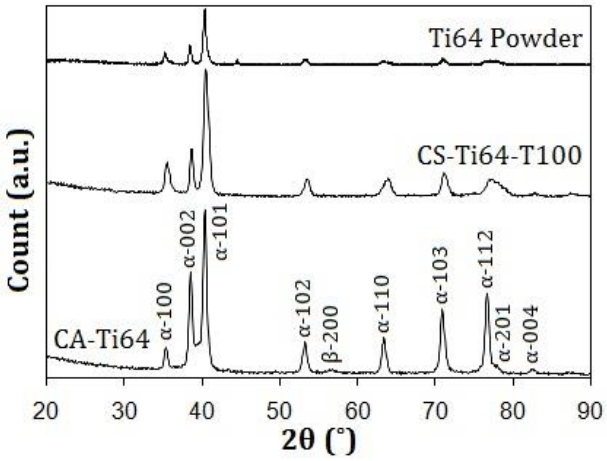

Figure 10. XRD patterns of CA-Ti64, CS-Ti64-T100, and Ti64 powder.

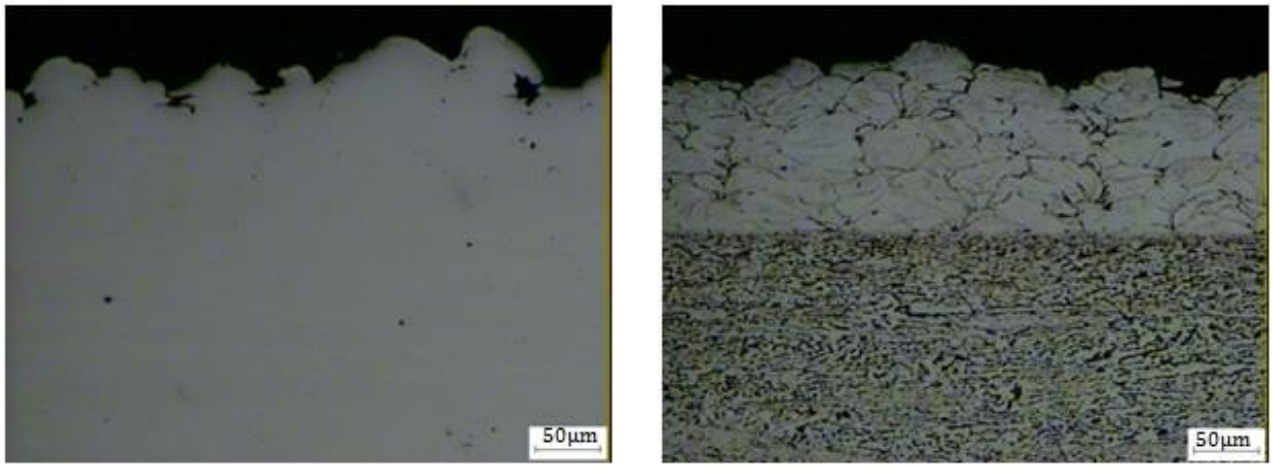

(a) (b)

Figure 11. Cross-sectional microstructures of CS-Ti64-T100 observed (a) before and (b) after etching.

Figures 11a and b show the cross-sectional microstructures of the CS-Ti64-T100 observed before and after etching, respectively. The comparison of these figures clearly shows that the detailed microstructure of the CS-Ti64-T100 with particle interfaces and a coating/substrate interface can be seen only after etching. Severely deformed Ti64 particles

can be clearly seen in the detailed microstructure of the CS-Ti64-T100 (Figure 11b) as no apparent gap between the CS-Ti64 coating and the CA-Ti64 substrate indicates a strong bonding between them [13]. It is clear that the kinetic energies of bombarding Ti64 particles during the CS deposition are sufficient to form their peripheries into jets and develop shear stresses in the regions where the particles are bonded on the substrate surface via adiabatic shear instability [15,16,20].

Figures 12a, b and c present the coating/substrate interfaces of the CS-Ti64-T100, CS-Ti64-T500, and CS-Ti64-T3000, respectively. Apparent interfacial gaps are not found for all the CS-Ti64 coatings, indicating their relatively strong bonding with their substrates [21]. Severely deformed Ti64 particles with a crescent shape can be seen in the cross-sectional microstructures of the CS-Ti64 coatings as pores can be found at interstitial sites between sprayed Ti64 particles.

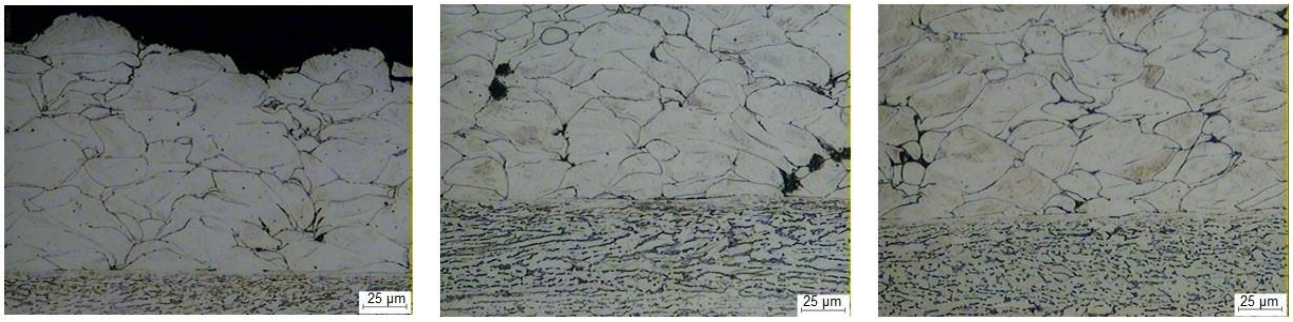

(a) (b) (c)

Figure 12. Cross-sectional microstructures with coating/substrate interfaces of (a) CS-Ti64-T100, (b) CS-Ti64-T500, and (c) CS-Ti64-T3000.

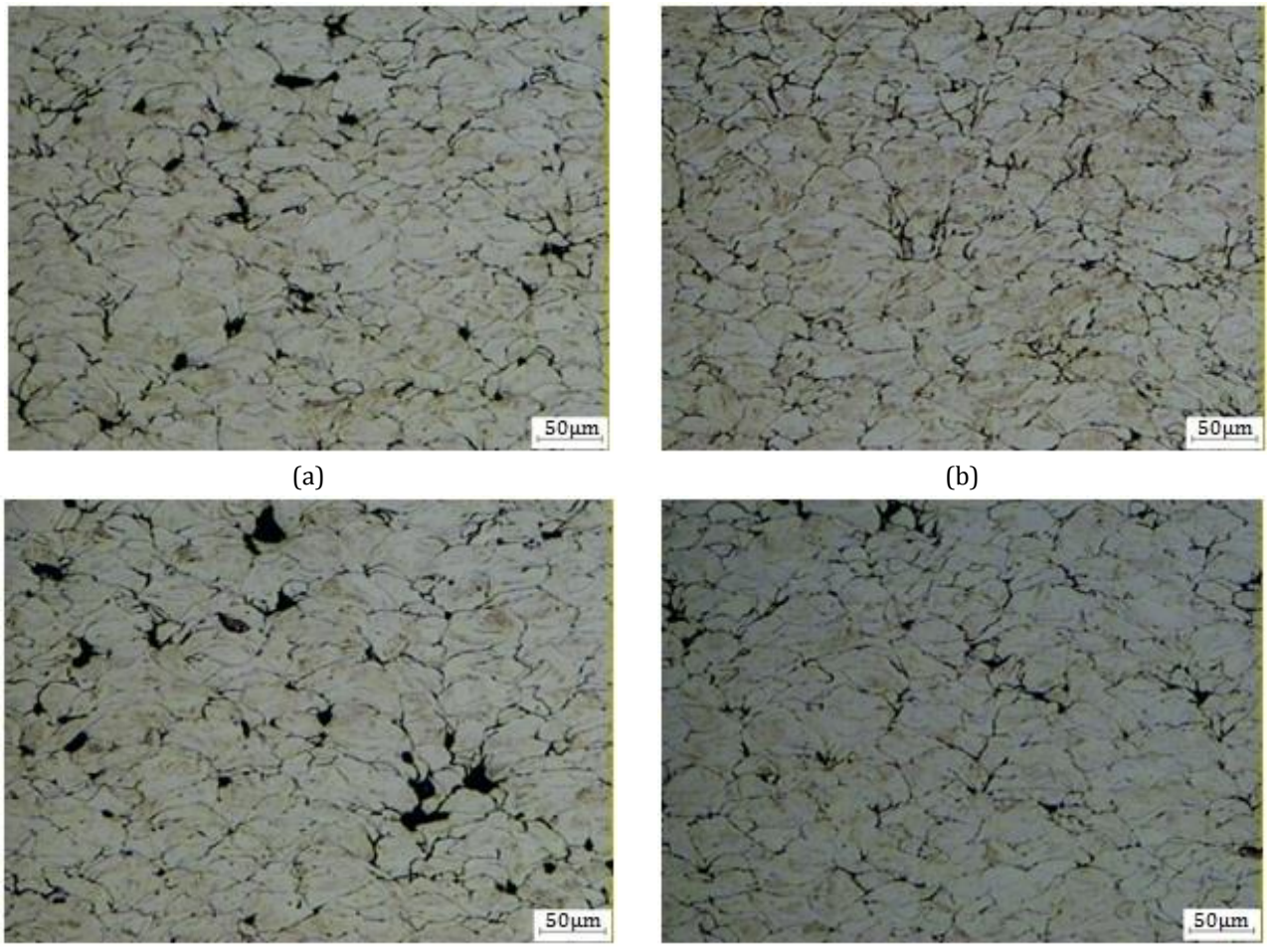

(a) (b)

(c) (d)

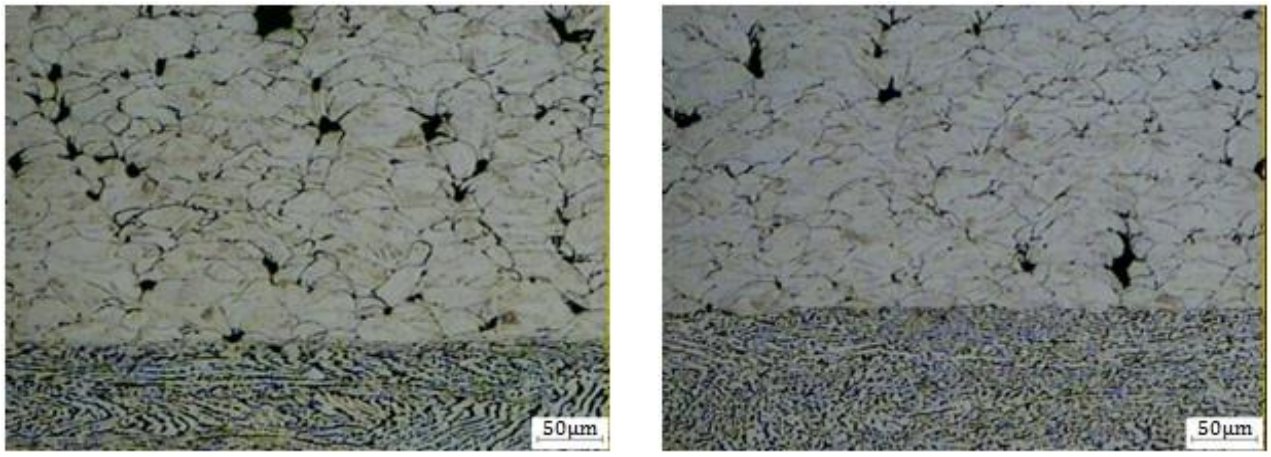

(e) (f)

Figure 13. Cross-sectional microstructures of (a, c and e) CS-Ti64-T1000 and (b, d and f) CS-Ti64-T3000 at different locations: (a and b) top, (c and d) centre, and (e and f) bottom including a coating/substrate interface.

Figure 13 shows the cross-sectional microstructures of the CS-Ti64-T1000 and CS-Ti64-T3000 at different locations. The CS-Ti64-T1000 and CS-Ti64-T3000 have severely deformed Ti64 particles in their cross-sectional microstructures as a certain number of pores is found throughout their CT. However, the CS-Ti64-T1000 has a larger number of pores left by unfilled gaps between sprayed Ti64 particles than the CS-Ti64-T3000, which is confirmed by the lower bulk porosity level (2±0.4%) of the CS-Ti64-T3000 than that (2.7±0.6%) of the CS-Ti64-T1000. It is therefore supposed that the longer high pressure CS deposition improves the bulk density of the CS-Ti64 coatings to a certain extent [8,11]. No apparent coating/substrate interfacial gaps are found for the both coatings as a result of their strong bonding with their substrates [21].

3.3 Analysis of surface and cross-sectional hardness

Figures 14a and b show the indents left on the cross-sections of the CA-Ti64 and CS-Ti64-T3000, respectively, after the indentations. All the indentations were carried out under the same conditions. Therefore, the smaller indent on the CS-Ti64-T3000 compared to that on the CA-Ti64 indicates its higher hardness and elastic modulus [21,22].

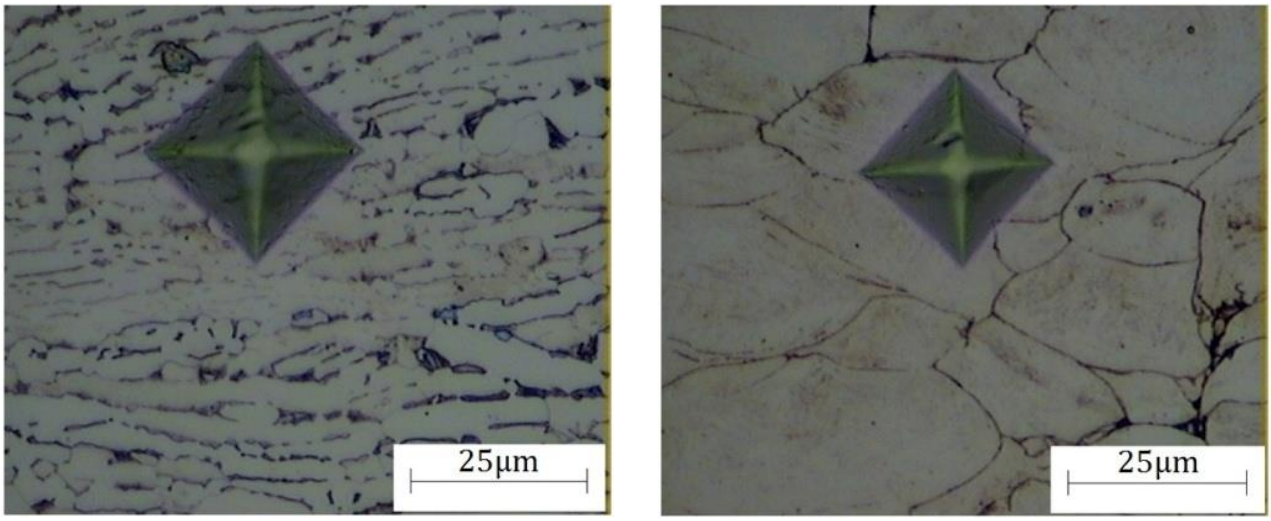

(a) (b)

Figure 14. Indents left on cross-sections of (a) CA-Ti64 and (b) CS-Ti64-T3000 after indentations.

Figures 15a, b, c, and d present the cross-sectional hardness of the CS-Ti64-T100, CS-Ti64-T500, CS-Ti64-T1000, and CS-Ti64-T3000, respectively. They all have higher hardness than their CA-Ti64 substrates as well as lower hardness at locations close to their surfaces since the less impinging effect of spray Ti64 particles prevents complete filling of gaps between sprayed Ti64 particles and gives rise to the higher surface porosity levels of the CS-Ti64 coatings [16,23]. Although they have relatively uniform hardness throughout their CT, especially for the thick coatings, a fluctuation in their hardness with respect to distance results from a non-uniform distribution of pores in their bulk structures [11,21,24]. The cross-sectional hardness of the CS-Ti64 coatings becomes higher throughout their CT with higher CT, as found in Figure 15, probably due to their lowered bulk porosity levels and pronounced cold work hardening associated with the longer high pressure CS deposition [2,25].

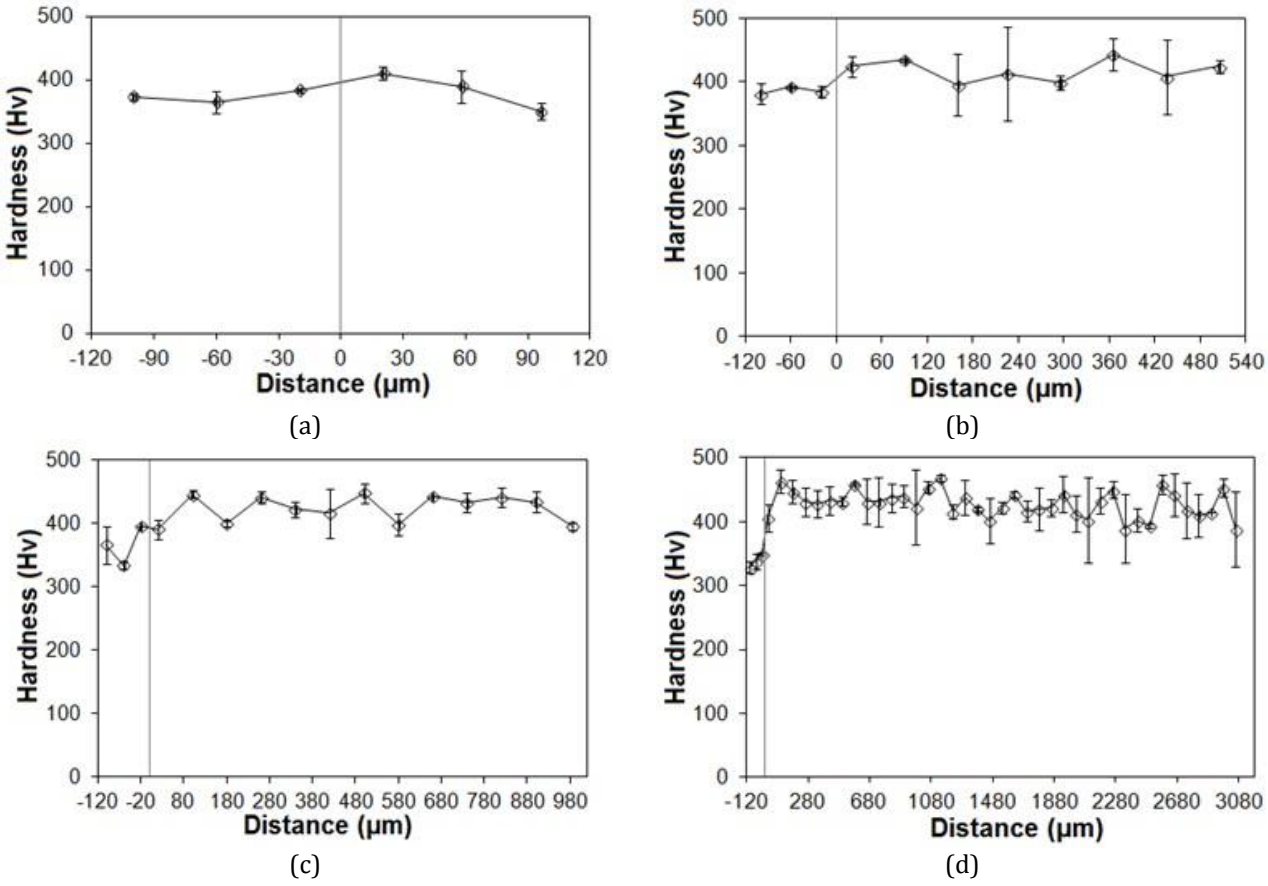

Figure 15. Cross-sectional hardness of (a) CS-Ti64-T100, (b) CS-Ti64-T500, (c) CS-Ti64-T1000, and (d) CS-Ti64-T3000. The lines represent coating/substrate interfaces.

Figure 16 presents the surface hardness of the CA-Ti64 and CS-Ti64 coatings with different CT. The CA-Ti64 has surface hardness of 371 Hv. The CS-Ti64-T100, CS-Ti64-T500, CS-Ti64-T1000, and CS-Ti64-T3000 have surface hardness of 400, 395, 409, and 410 Hv, respectively, indicating that their surface hardness consistently becomes higher with higher CT. The surface hardness of the CS-Ti64 coatings is apparently higher than that of the CA-Ti64 due to their cold work hardening associated with the high pressure CS deposition [2,11,17,18].

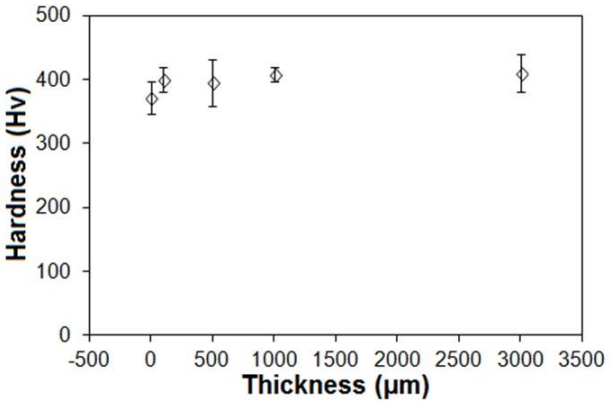

Figure 16. Surface hardness of CA-Ti64 and CS-Ti64 coatings with different CT.

3.4 Analysis of tensile bond strength

Figure 17 shows the graph of tensile bond strength versus extension of the CS-Ti64-T3000. The tensile bond strength of the CS-Ti64-T3000 is supposed to be more than 70 MPa since the tensile bond strength of the adhesive is about 70 MPa and the tensile bond failure has occurred only at the adhesive (Figure 5c) [13]. The other CS-Ti64 coatings also have similar tensile bond strength. It shows that the CS-Ti64 coatings have a relatively strong bonding with their CA-Ti64 substrates.

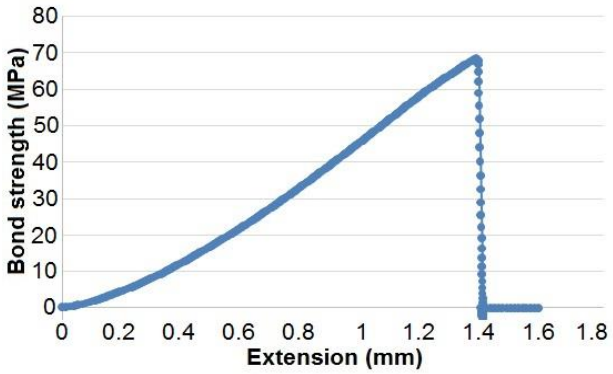

Figure 17. Tensile bond strength of CS-Ti64-T3000.

3.5. Analysis of wear and friction data

Figures 18a and b show the surface topographies of the polished CS-Ti64-T1000 and CS-Ti64-T3000, respectively. After the polishing, pores still can be found on their surface topographies since the intrinsic pores exist throughout the bulks of the coatings [26]. The R_q values of the polished CS-Ti64-T1000 and CS-Ti64-T3000 are 0.2±0.04 and 0.25±0.06 μm, respectively. All the tribo-tests were carried out on such coating surfaces.

Figure 19 presents the specific wear rates of the CA-Ti64 and CS-Ti64 coatings with different CT. The specific wear rate of the CA-Ti64 is 93.9×10^{-14} $m^3/(Nm)$. The specific wear rate of the CS-Ti64-T100 is 86.6×10^{-14} $m^3/(Nm)$, which is 7.8% lower than that of the CA-Ti64, indicating that the CS-Ti64-T100 has higher wear resistance as a result of its higher hardness [27-29]. The specific wear rates of the CS-Ti64-T500 and CS-Ti64-T1000 are 85.1×10^{-14} $m^3/(Nm)$ and 84.4×10^{-14} $m^3/(Nm)$, respectively. The specific wear rate of the CS-Ti64-T3000 is 78.1×10^{-14} $m^3/(Nm)$, which is 9.8% and 16.8% lower than those of the CS-Ti64-T100 and CA-Ti64, respectively. It indicates that the wear resistance of the CS-Ti64 coatings becomes higher with higher CT due to their higher hardness associated with the longer high pressure CS deposition as all the CS-Ti64 coatings used in this study have higher wear resistance than the CA-Ti64 as a result of their higher hardness attributed to their cold work hardening [2,11,17,18].

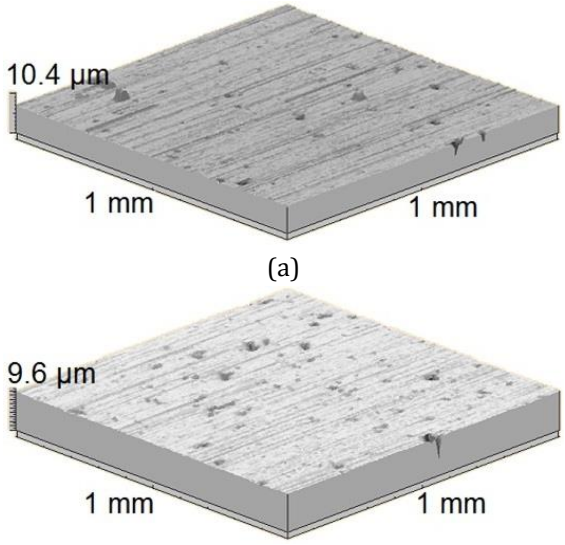

Figure 18. Surface topographies of polished CS-Ti64-T1000 and CS-Ti64-T3000.

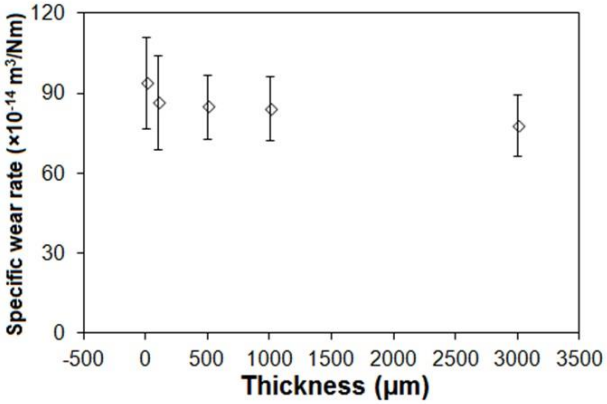

Figure 19. Specific wear rates of CA-Ti64 and CS-Ti64 coatings with different CT.

Figure 20a presents the friction coefficients of the CA-Ti64 and CS-Ti64 coatings with different CT against 100Cr6 steel. The friction coefficient of the CA-Ti64 is 0.55. The friction coefficient of the CS-Ti64-T100 is 0.57 that is slightly higher than that of the CA-Ti64. It is known that high interfacial shear strength between two rubbing surfaces in contact generates high friction

during a dry sliding process [2,11,28,30,31]. The high wear of rubbing surfaces lessens the interfacial shear strength by generating wear debris and releasing them into the interface and thereby reduces friction since wear debris can serve as spacers to prevent a direct contact between two rubbing surfaces and slide or roll under a lateral force [2,11,28,30,31]. In addition, roughening of rubbing surfaces via their wear can also reduce friction by lessening the interfacial shear strength [2,11,21,28]. Therefore, the lower wear of the CS-Ti64-T100 compared to that of the CA-Ti64 (Figure 20a) is responsible for its higher friction via less generation of wear debris and less roughening of its surface [2,11,21,28,30,31].

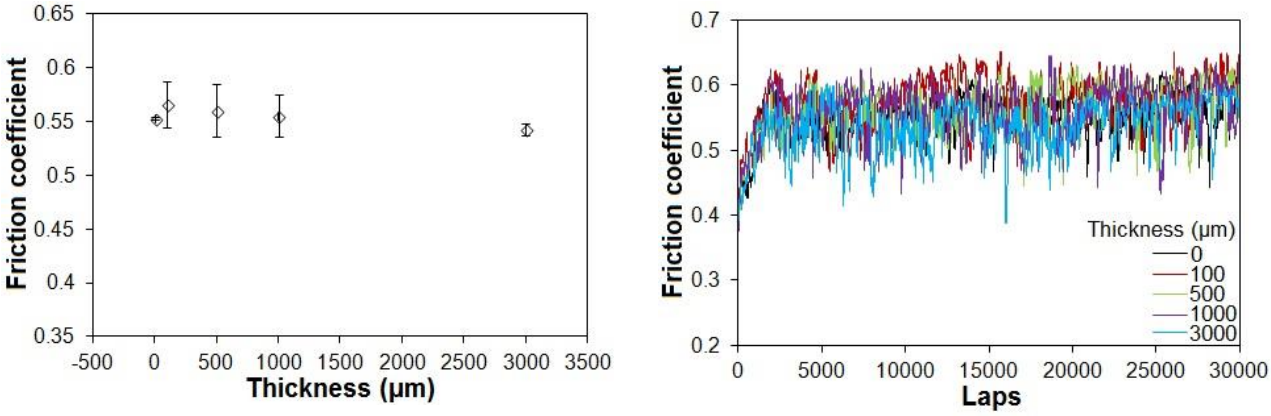

(a) (b)

Figure 20. Friction coefficients of CA-Ti64 and CS-Ti64 coatings as functions of (a) CT and (b) the number of laps.

A slight decrease in the friction of the CS-Ti64 coatings with increased CT is found in Figure 20a so that the friction coefficient of the CS-Ti64-T3000 is 0.54. The decreased wear of the CS-Ti64 coatings should increase their friction by decreasing generation of wear debris and roughening of their surfaces. However, the slightly decreased friction of the CS-Ti64 coatings with increased CT can be correlated to their decreased contact areas with their counter balls via their reduced wear since a larger contact between two rubbing surfaces can generate higher friction during a dry sliding process via a larger number of contact junctions between them [2,11,28-32].

Figure 20b illustrates the friction coefficients of the CA-Ti64 and CS-Ti64 coatings with different CT with respect to the number of laps. Although apparent fluctuations in the friction coefficients of the CA-Ti64 and CS-Ti64 coatings with respect to the number of laps are found as a result of the stick-slip phenomena [2,11,28,33], they all exhibit relatively stable friction during the entire dry sliding via their steady wear. The similar trends of friction coefficient versus laps of the CA-Ti64 and CS-Ti64 coatings can be understood with their similar wear behaviour against 100Cr6 steel.

3.6 Analysis of wear morphologies and topographies

Figure 21a, b, c, and d present the wear morphologies and topographies of the CA-Ti64, CS-Ti64-T100, CS-Ti64-T1000, and CS-Ti64-T3000, respectively. They all have apparent wear tracks as the wear track of the CS-Ti64 coatings becomes smaller with higher CT. The CA-Ti64 has a larger amount of wear debris on its wear track than the CS-Ti64 coatings, which is consistent with its lower friction. Under the not very much different generation of wear debris (Figures 21b, c and d), the smaller contact area of the thicker CS-Ti64 coating with its counter steel ball becomes the influential factor for its lower friction. Ploughed furrows on the wear tracks of the CA-Ti64 and CS-Ti64 coatings are indicative of their abrasive wear resulting from the repeated dry sliding of the steel balls on their surfaces [2,11,28,29,34]. The largest amount of generated wear debris on the wear track of the CA-Ti64 results in a formation of tribolayers by compacting them under the repeated sliding of the steel ball [2,11,28,35]. Such tribolayers are not apparently found on the wear tracks of the CS-Ti64 coatings with the less generation of wear debris associated with their higher wear resistance [2,11,28,35].

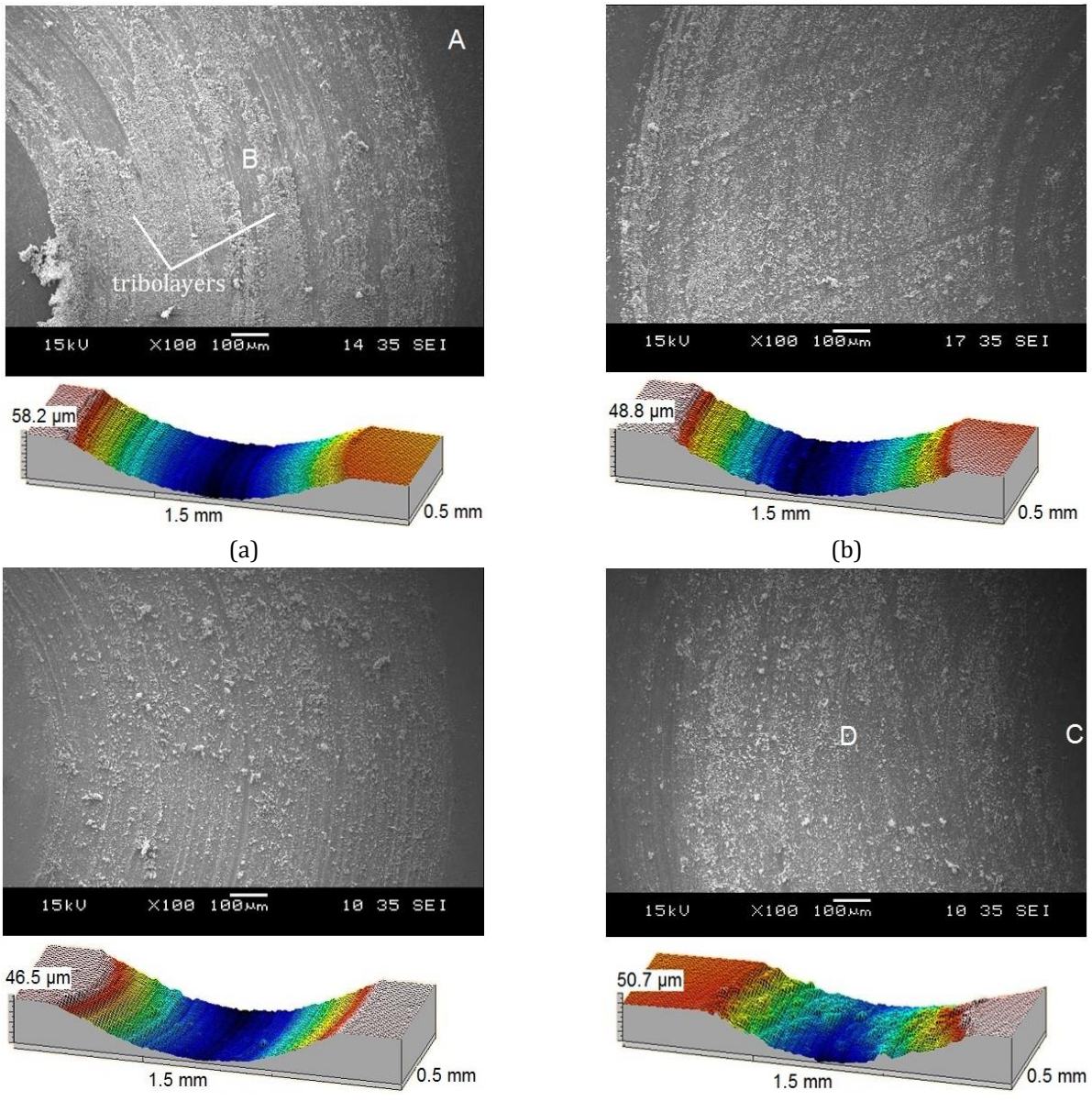

Figure 21. Wear morphologies (above) and topographies (below) of (a) CA-Ti64, (b) CS-Ti64-T100, (c) CS-Ti64-T1000, and (d) CS-Ti64-T3000.

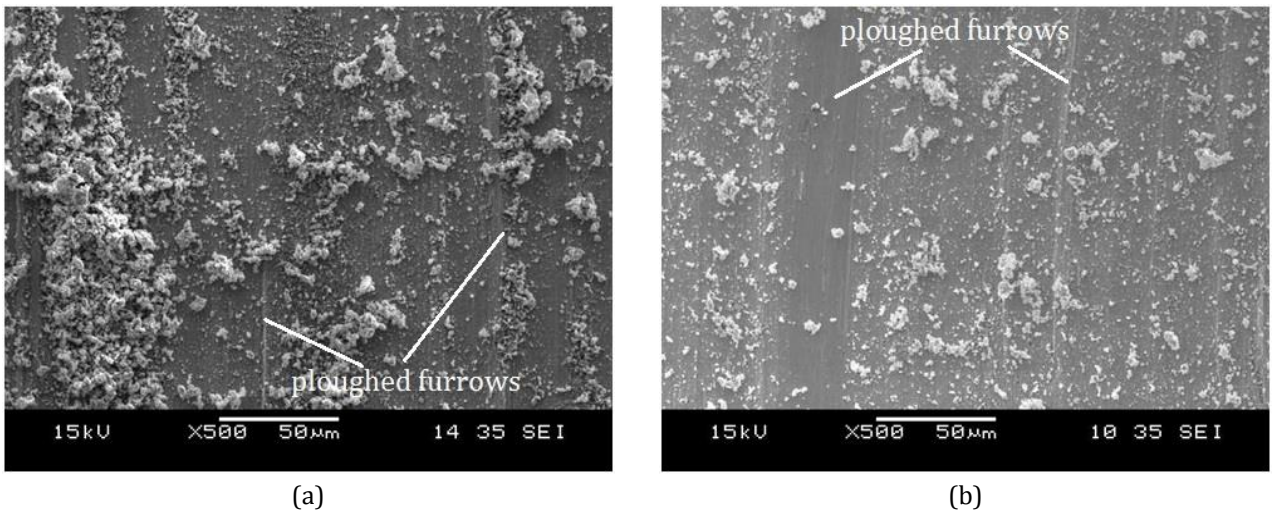

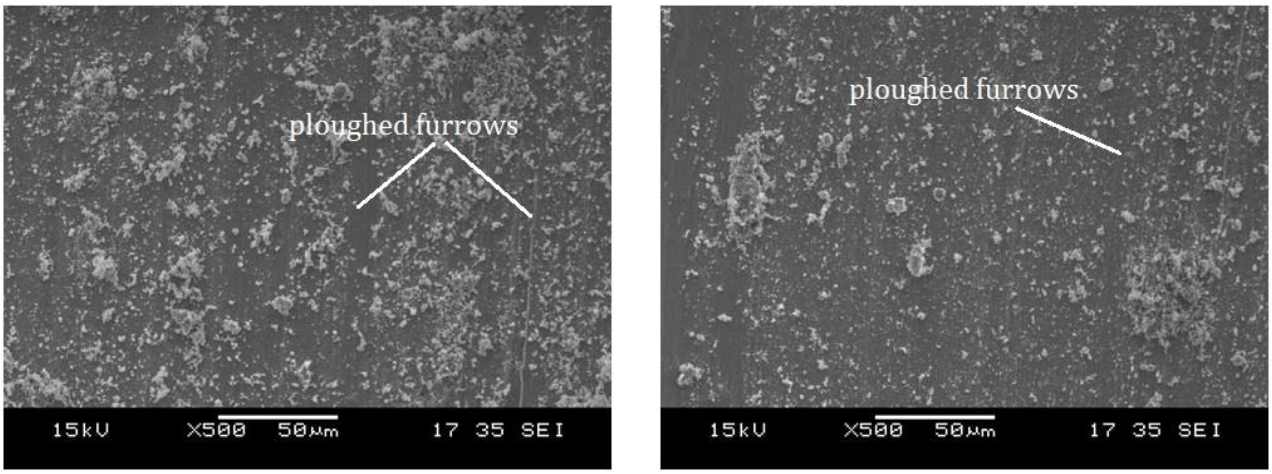

(c) (d)

Figure 22. Wear morphologies of (a) CS-Ti64-T100, (b) CS-Ti64-T500, (c) CS-Ti64-T1000, and (d) CS-Ti64-T3000 at higher magnification.

Figure 22 shows the wear morphologies of the CS-Ti64 coatings at the higher magnification. Ploughed furrows are clearly seen on their wear morphologies [2,11,28,29,34]. Normally, the repeated dry sliding of the steel ball initiates minute cracks at the interfaces between sprayed Ti64 particles and in the subsurface, propagates them along the interfaces and parallel to a free surface for some extent, and eventually results in a formation of interfacial micro-cracks and a removal of surface materials from deep regions as platelets, respectively [2,11,22,28,36]. The spallation of surface materials can be accelerated by the existence of weak interfacial bonds between sprayed Ti64 particles. However, no observation of interfacial micro-cracks and spallation on the wear tracks of all the CS-Ti64 coatings clearly indicates that the interfacial bond strength between sprayed Ti64 particles is strong enough to effectively eliminate their fatigue wear damages during the dry sliding. It clearly points out that the wear of the CS-Ti64 coatings is mainly attributed to their abrasive wear.

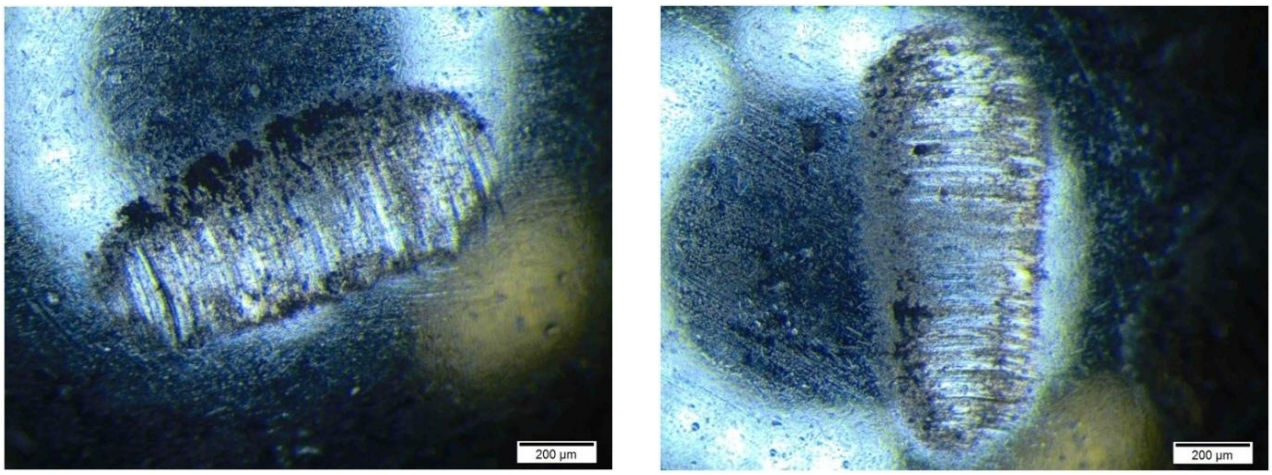

(a) (b)

Figure 23. Wear scars of 100Cr6 steel balls rubbed on (a) CA-Ti64 and (b) CS-Ti64-T3000.

Figures 23a and b show the wear scars of the 100Cr6 steel balls rubbed on the CA-Ti64 and CS-Ti64-T3000, respectively, on which abrasive lines apparently found can be correlated to their abrasive wear [2,11,28,29,34]. The wear scar of the 100Cr6 steel ball rubbed on the CS-Ti64-T3000 (1250 µm in length) is larger than that of the one rotated on the CA-Ti64 (1176.5 µm in length) because the higher wear resistance of the CS-Ti64-T3000 results in the higher wear of its counter steel ball.

3.7 Chemical analysis of surface wear and wear debris

Figures 24a and b show the EDX spectra of the CA-Ti64 measured on its untested area and wear track, respectively, with the four major peaks of Ti, Al, V and C elements although the EDX spectrum measured on its wear track has an additional O peak associated with an occurrence of an oxidation process during the dry sliding [2,11,28,37]. The C peak is attributed to surface carbon contaminants adsorbed after exposure to air wherewith the Ti, Al and V peaks result from the Ti64 matrix [2,11,28,38]. The EDX spectra of the CS-Ti64-T3000 measured on its untested area and wear track are presented in Figures 24c and d, respectively. The CS-Ti64-T3000 (Figures 24c and d) has the similar EDX spectra to those of the CA-Ti64 (Figures 24a and b), indicating that they have similar wear mechanisms against 100Cr6 steel under the dry condition. The O peak on the EDX spectrum measured on the wear track of the CS-Ti64-T3000 (Figure 24d) indicates the occurrence of a dry sliding induced oxidation process [2,11,28].

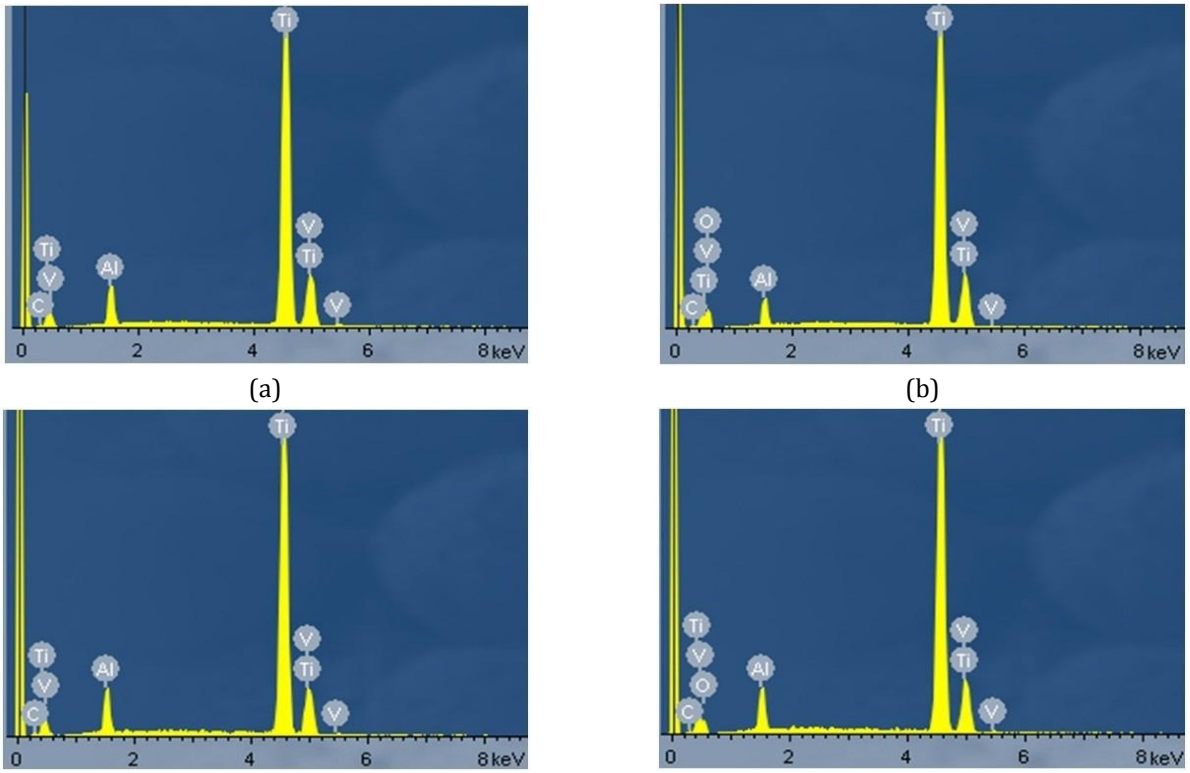

Figure 24. EDX spectra of (a and b) CA-Ti64 and (c and d) CS-Ti64-T3000 measured at locations (a) "A" in untested area and (b) "B" in wear track of Figure 21a and (c) "C" in untested area and (d) "D" in wear track of Figure 21d.

Figure 25 shows an overview of wear debris found on the wear track of the CS-Ti64-T3000. The irregular shaped wear debris are indicative of tearing and break-in wear caused by the surface asperities of the hard steel ball [2,11,28,39].

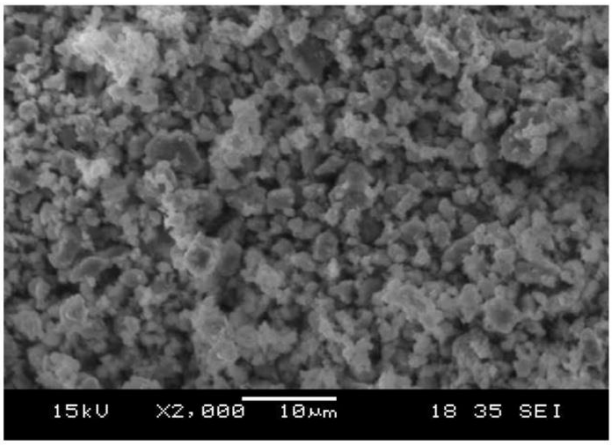

Figure 25. An overview of wear debris found on wear track of CS-Ti64-T3000.

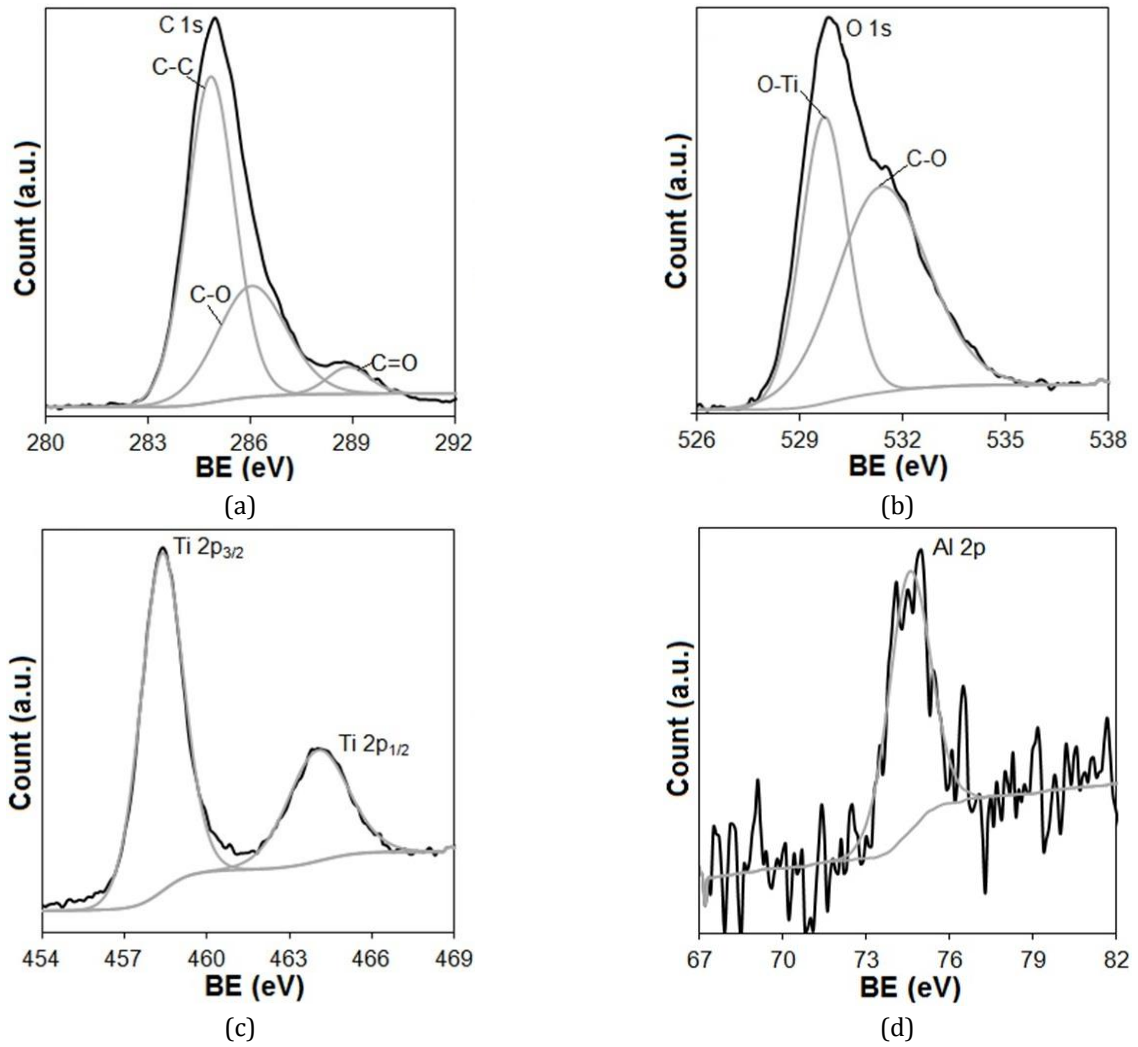

Figure 26. Fitted XPS spectra of wear debris of CS-Ti64-T3000 in Figure 25: (a) C 1s, (b) O 1s, (c) Ti 2p, and (d) Al 2p.

Figures 26a, b, c, and d show the fitted XPS C 1s, O 1s, Ti 2p and Al 2p peaks of the wear debris of the CS-Ti64-T3000 in Figure 25, respectively. The deconvolution of the peaks was carried out with a Gaussian line shape and a Shirley background. In Figure 26a, the C 1s peak is deconvoluted into three components assigned to C-C bonds (full-width-half-maximum (FWHM)= 1.65 eV) at 284.8 eV, C-O bonds (FWHM= 2.4 eV) at 286 eV, and C=O bonds (FWHM= 1.46 eV) at 288.9 eV [11,40]. In Figure 26b, the O 1s peak is mainly composed of two components attributed to O-Ti bonds (FWHM= 1.59 eV) at 529.7 eV and C-O bonds (FWHM= 3.13 eV) at 531.4 eV [11,41]. The component of the O 1s peak at 531.4 eV can also be attributed to oxidized Al [11,40]. Two spin-orbit coupling peaks of the Ti 2p are recorded at 458.3 eV for the Ti $2p_{3/2}$ peak (FWHM= 1.82 eV) and at 464 eV for the Ti $2p_{1/2}$ peak (FWHM= 2.58 eV) as found in Figure 26c. The existence of the Al 2p peak (FWHM= 1.76 eV) at 74.5 eV is an indication of oxidized Al (Figure 26d) [40,41]. The V element is not apparently detected in the wear debris. The XPS results clearly show that the wear debris of the CS-Ti64-T3000 are significantly oxidized.

4. CONCLUSIONS

The CS-Ti64 coatings with different CT of 100-3000 μm were deposited on the CA-Ti64 substrates using a high pressure CS system. Their structural, mechanical and tribological properties were systematically investigated.

- The bulk porosity levels of the CS-Ti64 coatings were lower with higher CT, indicating their improved bulk densities associated with the longer high pressure CS deposition.

- No apparent gaps between the CS-Ti64 coatings and the CA-Ti64 substrates were found as a result of the strong bonding between them. The tensile bond strength tests confirmed that the CS-Ti64 coatings had a relatively strong bonding with their CA-Ti64 substrates.
- The hardness of the CS-Ti64 coatings was higher with higher CT due to their lowered bulk porosity levels and pronounced cold work hardening as their hardness was higher than that of the CA-Ti64 because of their cold work hardening.
- The increased CT from 100 to 3000 μm resulted in a 9.8% decrease in the specific wear rates of the CS-Ti64 coatings as a result of their increased hardness as the specific wear rate of the CS-Ti64-T3000 was 16.8% lower than that of the CA-Ti64. The higher hardness of the CS-Ti64 coatings than that of the CA-Ti64 resulted in their lower specific wear rates for all the CT. It was clear that the CS-Ti64 coatings had higher abrasive wear resistance than the CA-Ti64.
- The prolonged high pressure CS deposition for the thick CS-Ti64 coatings had an influence on the porosity, hardness, and abrasive wear resistance of the CS-Ti64 coatings.

Acknowledgement

Authors are grateful for the financial support from the National Research Foundation (NRF), Rolls-Royce (RR), and Nanyang Technological University (NTU), Singapore, with the NRF-RR-NTU research grant number of M-RT3.1, and the project team members from RR, Singapore, Harry Eyre, Anna Tai, and Nicholas Weeks for their contributions in this work.

ORCID iDs

Nay Win Khun 0000-0002-5209-020X
Adrian Wei Yee Tana 0000-0002-8449-5500
Wen Sun 0000-0002-7589-6804
Erjia Liu 0000-0003-3231-455X

REFERENCES

[1] H. Singh, T. S. Sidhu, and S. B. S. Kalsi, "Cold spray technology: Future of coating deposition processes," *Frattura ed Integrità Strutturale*, vol. 22, pp. 69-84, Oct. 2012, doi: 10.3221/IGF-ESIS.22.08.

[2] N. W. Khun, P. Q. Trung, A. W. Y. Tan, S. Wen, E. Liu, and D. L. Butler, "Effects of shot peening pressure on friction and wear of high pressure cold sprayed Ti-6Al-4V coatings under dry and lubrication conditions," *Tribology in Industry*, vol. 45, no. 3, pp. 472-486, Sep. 2023, doi: 10.24874/ti.1466.03.23.05.

[3] W. Hu, S. Markovych, K. Tan, O. Shorinov, and T. Cao, "Surface repair of aircraft titanium alloy parts by cold spraying technology," *Aerospace Technic and Technology*, vol. 3, pp. 30-42, Mar. 2020, doi: 10.32620/aktt.2020.3.04.

[4] B. Song, M. Bai, K. T. Voisey, and T. Hussain, "Role of oxides and porosity on high temperature oxidation of liquid fueled HVOF thermal sprayed Ni50Cr coatings," *Journal of Thermal Spray Technology*, vol. 26, pp. 554-568, Jan. 2017, doi: 10.1007/s11666-017-0531-z.

[5] S. B. Pitchuka, B. Boesl, C. Zhang, D. Lahiri, A. Nieto, G. Sundararajan, and A. Agarwal, "Dry sliding wear behavior of cold sprayed aluminum amorphous/nanocrystalline alloy coatings," *Surface and Coatings Technology*, vol. 238, pp. 118-125, Jan. 2014, doi: 10.1016/j.surfcoat.2013.10.055.

[6] K. Spencer, D. Fabijanic, and M. X. Zhang, "Cold spray of Al-MMC coatings on magnesium alloys for improved corrosion and wear resistance," *Materials Science Forum*, vol. 618-619, pp. 377-380, Apr. 2009, doi: 10.4028/www.scientific.net/MSF.618-619.377.

[7] G. D. Revankar, R. Shetty, S. S. Rao, and V. N. Gaitonde, "Wear resistance enhancement of titanium alloy (Ti6Al4V) by ball burnishing process," *Journal of Materials Research and Technology*, vol. 6, no. 1, pp. 13-32, Mar. 2017, doi: 10.1016/j.jmrt.2016.03.007.

[8] M. Ashokkumar, D. Thirumalaikumarasamy, T. Sonar, S. Deepak, P. Vignesh, and M. Anbarasu, "An overview of cold spray coating in additive manufacturing, component repairing and other engineering applications," *Journal of the Mechanical Behaviour of Materials*, vol. 31, pp. 514-534, July 2022, doi: 10.1515/jmbm-2022-0056.

[9] A. Moridi, S. M. H. Gangaraj, S. Vezzu, and M. Guagliano, "Number of passes and thickness effect on mechanical characteristics of cold sprayed coating," *Procedia Engineering*, vol. 74, pp. 449-459, June 2014, doi: 10.1016/j.proeng.2014.06.296.

[10] Y. Xiong, W. Zhuang, and M. X. Zhang, "Effect of the thickness of cold sprayed aluminium alloy coating on the adhesive bond strength with an aluminium alloy substrate," *Surface and Coatings Technology*, vol. 270, pp. 259-265, May 2015, doi: 10.1016/j.surfcoat.2015.02.048.

[11] N. W. Khun, A. W. Y. Tan, and E. Liu, "Mechanical and tribological properties of cold sprayed Ti coatings on Ti6Al4V substrates," *Journal of Thermal Spray Technology*, vol. 25, no. 4, pp. 715-724, Mar. 2016, doi: 10.1007/s11666-016-0396-6.

[12] J. J. H. McCallister, M. D. Gammage, J. W. Keto, M. F. Becker, and D. Kovar, "Influence of agglomerate morphology on micro cold spray of Ag nanopowders", *Journal of Aerosol Science*, vol. 151, pp. 105648, Jan. 2021, doi: 10.1016/j.jaerosci.2020.105648.

[13] D. Boruah, B. Robinson, T. London, H. Wu, H. D. V. Lovelock, P. McNutt, M. Dore, and X. Zhang, "Experimental evaluation of interfacial adhesion strength of cold sprayed Ti6Al4V thick coatings using an adhesive free test method," *Surface and Coatings Technology*, vol. 381, pp. 125130, Jan. 2020, doi: 10.1016/j.surfcoat.2019.125130.

[14] H. Assadi, F. Gartner, T. Stoltenhoff, and H. Kreye, "Bonding mechanism in cold gas spraying", *Acta Materials*, vol. 51, pp. 4379-4394, Sep. 2003. doi: 10.1016/S1359-6454(03)00274-X.

[15] M. A. A. Nyiak and A. A. Tiamiyu, "Recent advances on bonding mechanisms in cold spray process: A review of single particle impact methods," *Journal of Materials Research*, vol. 38, pp. 69-95, Jan. 2023, doi: 10.1557/s43578-022-00764-2.

[16] A. W. Y. Tan, W. Sun, A. Bhowmik, J. Y. Lek, L. Marinescu, F. Li, N. W. Khun, Z. Dong, and E. Liu, "Effect of coating thickness on microstructure, mechanical properties and fracture behaviour of cold sprayed Ti6Al4V coatings on Ti6Al4V substrates," *Surface and Coatings Technology*, vol. 349, pp. 303-317, Sep. 2018, doi: 10.1016/j.surfcoat.2018.05.060.

[17] Y. Chong, T. Bhattacharjee, and N. Tsuji, "Bi-lamellar microstructure in Ti-6Al-4V: Microstructure evolution and mechanical properties," *Materials Science and Engineering A*: vol. 762, pp. 138077, Aug. 2019, doi: 10.1016/j.msea.2019.138077.

[18] V. S. Bhattiprolu, K. W. Johnson, and G. A. Crawford, "Influence of powder microstructure on the microstructural evolution of as-sprayed and heat treated cold sprayed Ti6Al4V coatings," *Journal of Thermal Spray Technology*, vol. 28, pp. 174-188, Jan. 2019, doi: 10.1007/s11666-018-0812-1.

[19] J. M. Oh, B. G. Lee, S. W. Cho, S. W. Lee, G. S. Choi, and J. W. Lim, "Oxygen effects on the mechanical properties and lattice strain of Ti and Ti6Al4V," *Metals and Materials International*, vol. 17, pp. 733-736, Oct. 2011, doi: 10.1007/s12540-011-1006-2.

[20] R. E. Blose, B. H. Walker, R. M. Walker, and S. H. Froes, "New opportunities to use cold spray process for applying additive features to titanium alloys," *Metal Powder Report*, vol. 61, no. 9, pp. 30-37, Oct. 2006. doi: 10.1016/S0026-0657(06)70713-5.

[21] L. He and M. Hassani, "A review of the mechanical and tribological behaviour of cold spray metal matrix composites," *Journal of Thermal Spray Technology*, vol. 29, pp. 1565-1608, Sep. 2020, doi: 10.1007/s11666-020-01091-w.

[22] P. Poza and M. A. G. Maneiro, "Cold spray coatings: Microstructure, mechanical properties, and wear behaviour," *Progress in Materials Science*, vol. 123, pp. 100839, Jan. 2022, doi: 10.1016/j.pmatsci.2021.100839.

[23] T. H. V. Steenkiste, J. R. Smith, and R. E. Teets, "Aluminium coatings via kinetic spray with relatively large powder particles," *Surface and Coatings Technology*, vol. 154, no. 2-3, pp. 237-252, May 2002. doi: 10.1016/S0257-8972(02)00018-X.

[24] D. Goldbaum, J. Ajaja, R. R. Chromik, W. Wong, S. Yue, E. Irissou, and J. G. Legoux, "Mechanical behaviour of Ti cold spray coatings coatings determined by a multi-scale indentation method," *Materials Science and Engineering A*, vol. 530, pp. 253-265, Dec. 2011, doi: 10.1016/j.msea.2011.09.083.

[25] D. Klenam, T. Asumadu, M. Bodunrin, M. Vandadi, T. Bond, J. V. D. Merwe, N. Rahbar, and W. Soboyejo, "Cold spray coatings of complex concentrated alloys: critical assessment of milestones, challenges, and opportunities," *Coatings*, vol. 13, no. 3, pp. 538, Mar. 2023, doi: 10.3390/coatings13030538.

[26] Y. Y. Wang, J. Adrien, and B. Normand, "Porosity characterization of cold spray stainless steel coatings using three dimensional X ray microtomography," *Coatings*, vol. 8, no. 9, pp. 326, Sep. 2018, doi: 10.3390/coatings8090326.

[27] H. Bai, L. Zhong, L. Kang, J. Liu, W. Zhuang, Z. Lv, and Y. Xu, "A review on wear resistant coating with high hardness and high toughness on the surface of titanium alloy," *Journal of Alloys and Compounds*, vol. 882, pp. 160645, Nov. 2021, doi: 10.1016/j.jallcom.2021.160645.

[28] N. W. Khun, W. Q. Toh. and E. Liu, "Study on changes in hardness and wear resistance of 3D printed Ti-6Al4-V with respect to heat treatment temperature," *Tribology in Industry*, vol. 45, no. 1, pp. 129-135, Mar. 2023, doi: 10.24874/ti.1421.12.22.02.

[29] R. B. Nair, S. Ngan, and A. McDonald, "Dry abrasive wear wear and solid particle erosion assements of high entropy alloy coatings fabricated by cold spraying," *Materialstoday Communications*, vol. 34, pp. 105527, Mar. 2023, doi: 10.1016/j.mtcomm.2023.105527.

[30] X. He, Z. Liu, L. B. Ripley, V. L. Swensen, I. J. G. Wiesner, B. R. Gulner, G. R. McAndrews, R. J. Wieser, B. P. Borovsky, Q. J. Wang, and S. H. Kim, "Empirical relationship between interfacial shear stress and contact pressure in micro and macro scale friction," *Tribology International*, vol. 155, pp. 106780, Mar. 2021, doi: 10.1016/j.triboint.2020.106780.

[31] M. M. Khrushchev, "Principal of abrasive wear," *Wear*, vol. 28, no. 1, pp. 69–88, Apr. 1974, doi: 10.1016/0043-1648(74)90102-1.

[32] X. M. Liang, Y. Z. Xing, L. T. Li, W. K. Yuan, and G. F. Wang, "An experimental study on the relation between friction force and real contact area," *Scientific Reports*, vol. 11, no. 20366, Oct. 2021, doi: s41598-021-99909-2.

[33] J. Awrejcewicz and P. Olejnik, "Occurrence of stick-slip phenomenon," *Journal of Theoretical Applied Mechanics*, vol. 45, no. 1, pp. 33-40, 2007. doi: v45n1p33.

[34] C. J. Akisin, F. Venturi, M. Bai, C. J. Bennett, and T. Hussain, "Microstructure, mechanical and wear resistant properties of low pressure cold spayed Al-7Mg/Al_2O_3 and Al-10Mg/Al_2O_3 composite coatings," *Emergent Materials*, vol. 4, pp. 1569-1581, Sep. 2021, doi: 10.1007/s42247-021-00293-4.

[35] V. N. V. Munagala and R. R. Chromik, "The role of metal powder properties on the tribology of cold sprayed Ti6Al4V-TiC metal matrix composites," *Surface and Coatings Technology*, vol. 411, pp. 126974, Apr. 2021, doi: 10.1016/j.surfcoat.2021.126974.

[36] S. Stewart and R. Ahmed, "Rolling contact fatigue of surface coatings: A review," *Wear*, vol. 253, no. 11-12, pp. 1132-1144, Dec. 2002, doi: 10.1016/S0043-1648(02)00234-X.

[37] L. D. Conceicao and A. S. C. M. DOliveira, "The effect of oxidation on the tribolayer and sliding wear of a Co-based coating," *Surface and Coatings Technology*, vol. 288, pp. 69-78, Feb. 2016, doi: 10.1016/j.surfcoat.2016.01.013.

[38] R. Hayashi, T. Ueno, S. Migita, Y. Tsutsumi, H. Doi, T. Ogawa, T. Hanawa, and N. Wakabayashi, "Hydrocarbon deposition attenuates osteoblast activity on titanium," *Journal of Dental Research*, vol. 93, no. 7, pp. 698-703, May 2014, doi: 10.1177%2F0022034514536578.

[39] M. J. Nine, D. Choudhury, A. C. Hee, R. Mootanah, and N. A. A. Osman, "Wear debris characterization and corresponding biological response: Artificial hip and knee joints," *Materials*, vol. 7, no. 2, pp. 980-1016, Feb. 2014, doi: 10.3390%2Fma7020980.

[40] N. Derimow, J. M. Gorham, M. L. Martin, J. T. Benzing, R. M. White, and N. Hrabe, "Surface chemistry in Ti-6Al-4V feedstock as influenced by powder reuse in electron beam additive manufacturing," *Applied Surface Science*, vol. 602, pp. 154280, Nov. 2022, doi: 10.1016/j.apsusc.2022.154280.

[41] P. C. Snijiders, L. P. H. Jeurgens, and W. G. Sloof, "Structure of thin aluminum-oxide films determined from valence band spectra measured using XPS," *Surface Science*, vol. 496, no. 1-2, pp. 97-109, Jan. 2002, doi: 10.1016/S0039-6028.